ACS APPLIED MATERIALS & INTERFACES

Research Article

www.acsami.org

Contrast Enhanced Microscopy Digital Image Correlation: A General Method to Contact-Free Coefficient of Thermal Expansion Measurement of Polymer Films

Jairo A. Diaz,[†] Robert J. Moon,[‡] and Jeffrey P. Youngblood*,[†]

[†]School of Materials Engineering, Purdue University, 701 West Stadium Avenue, West Lafayette, Indiana 47907, United States

[‡]Forest Products Laboratory, U.S. Forest Service, One Gifford Pinchot Drive, Madison, Wisconsin, 53726, United States

Supporting Information

ABSTRACT: Thermal expansion represents a vital indicator of the processing history and dimensional stability of materials. Solvent-sensitive, thin, and compliant samples are particularly challenging to test. Here we describe how textures highlighted by contrast enhanced optical microscopy modes (i.e., polarized light (PL), phase contrast (PC)) and bright field (BF) can be used to determine the thermal expansion of polymer films in a contact-free way using digital image correlation (DIC). Three different films were explored: polyetherimide (PEI), polyimide (PI), and polyethylene naphthalate (PEN). Image textural features (e.g., intensity, size, speckle pattern characteristics) obtained by BF, PC, and PL were analyzed by two-dimensional Fourier transform and autocorrelations. The measured in-plane CTEs of PEI, PI, and PEN films, 51.8, 20.5, and 10.2 ppm/K, respectively, closely approached those previously reported using DIC with artificially applied speckle patterns.

KEYWORDS: *polymer films, phase contrast, polarized light, image analysis, coefficient of thermal expansion, digital image correlation*

INTRODUCTION

Thermal dimensional stability in soft materials is a matter of paramount importance during materials characterization and performance in different application fields such as biomaterials and organic electronics; nonetheless, the measurement of thermal strain is challenging due to the typically temperature-dependent stiffness and complex geometric configurations exhibited by soft samples. Under such conditions a contact-free testing method is highly recommended to properly monitor their molecular and structural response to thermal loads without altering the structure or hindering the free expansion of the samples. For self-standing polymeric films with thicknesses on the order of micrometers, in spite of the numerous methods available for thermal expansion measurement only a few could be employed as shown in Figure 1. Digital image correlation (DIC) becomes very advantageous over other contact-free methods like ellipsometry or electronic speckle pattern interferometry (ESPI), since it does not require the analysis of generated fringes, and retains good resolution with full field strain determination at different length scales. DIC relies on the efficient cross-correlation of images containing distinctive trackable patterns taken at different times, as subjected to different temperatures in the case of thermal strain determination. Such patterns are typically introduced by paint spraying, coating, or physically modifying the surface of testing specimens.[1] Finely distributed patterns have also been obtained in samples at lower length scales by depositing 5 μm titanium particles via vacuum sputtering,[2] metallic thin films via chemical vapor deposition[3] or solution depositing rhodamine B isothiocyanate labeled silica nanoparticles.[4] The capabilities of DIC measurements have been further extended by tracking nanoscale patterns identified by

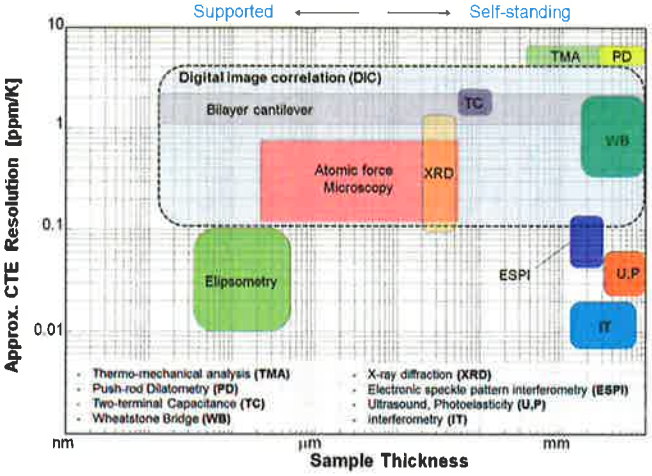

Figure 1. Common methods employed in thermal expansion determination as a function of sample thickness. Samples with thickness below ~5 μm are typically tested on a substrate (Supported) as opposite to thicker, non-supported samples (Self-standing).[8−28]

Received: December 18, 2013
Accepted: March 20, 2014
Published: March 20, 2014

Table 1. Comparison of CTEs for PI, PEI, and PEN Films

material	method	CTE [ppm/K]	temp. range [°C]	image characteristics	ref
Polyimide (PI)	DIC - Bright Field	CTE*x*: 18.0 ± 3.2 CTE*y*: 22.0 ± 3.2	30−100	Fine texture, low contrast, HWHM: 4.4 ± 1.2	This work
	DIC - Phase Contrast	CTE*x*: 18.8 ± 3.4 CTE*y*: 21.4 ± 2.6	30−100	Fine texture, high contrast, HWHM: 6.3 ± 0.7	This work
	DIC - Polarized Light	CTE*x*: 22.9 ± 2.2 CTE*y*: 19.6 ± 0.2	30−100	Fine texture, low contrast, HWHM: 5.8 ± 1.0	This work
	DIC - Paint Spray	CTE: 16.85 ± 1.0	30−100	Stochastic, artificial speckle pattern	13
	ASTM D-696-91	CTE: 17−20	−14 to 38	NA	52
Polyether-imide (PEI)	DIC- Bright Field	CTE*x*:[a] 50.9 ± 3.4	30−100	Granular-like texture, low contrast, HWHM: 10.3 ± 0.5	This work
	DIC - Phase Contrast	CTE*x*: 52.1 ± 2.4 CTE*y*: 51.9 ± 3.9	30−100	Sparsely distributed, random spots, HWHM: 13.8 ± 2.2	This work
	DIC - Polarized Light	CTE*x*: 53.0 ± 2.6 CTE*y*: 52.1 ± 3.9	30−100	Narrow distribution random speckle, HWHM: 10.9 ± 0.2	This work
	DIC - Paint Spray	CTE: 50.92 ± 2.0	30−100	Stochastic, artificial speckle pattern	13
	IPC-TM-650	CTE: 52	-	NA	53
Polyethylene Naphthalate (PEN)	DIC - Phase Contrast	CTE*x*: 10.2 ± 1.8 CTE*y*: 10.2 ± 2.5	30−70	Broad distribution spaced speckles, HWHM: 15.3 ± 1.7	This work
	DIC - Paint Spray	CTE*x*: 13.42 CTE*y*: 13.88	30−120	Stochastic, artificial speckle pattern	15
	Thermomechanical Analysis (TMA)	CTE*x*: 11 18 CTE*y*: 16 - 18	0−100	NA	45

[a]Free expansion in perpendicular direction hindered by friction, CTE_y < 20 ppm/K.

scanning electron microscopy (SEM)[5] and atomic force microscopy (AFM).[6,7]

Despite the number of patterning methods employable for DIC samples, the pattern generation process can still be very challenging for highly sensitive systems (e.g., solvent-sensitive, highly compliant, or brittle films) that only allow minimal external contact. Any thermal, chemical, or mechanical exposure of the testing samples during pattern preparation not only suppresses the contact-free nature of the method, but also, if not applied properly (i.e., weak particle adhesion, defect generation, etc.), could affect the sample integrity and the stability of measurements. Nevertheless, materials have various types of structural features (e.g., surface roughness, defects, crystallinity, coatings, impurities, orientations, etc.) developed during self-assembly, processing history, or manipulation, which can be employed together with DIC for strain measurements.[2,29−31] Recent studies have employed polarized light to enhance image contrast and measure strains via DIC in sensitive systems such as cellulose nanocrystal films[16] and a bat wing skin.[32] The remarkable roles played by phase contrast on cell biology and polarized light in the study of liquid crystals and minerals led us to explore their potentials as practical contrast enhancing methods to generate acceptable trackable patterns from polymer films to perform measurements via DIC.

Hereby, we study how natural structural features present in high-performance commercial polyetherimide (PEI), polyimide (PI), and polyethylene naphthalate (PEN) films as imaged by bright field (BF), phase contrast (PC), and polarized light (PL) microscopy can produce images that exhibit textural features (e.g., fine, contrast enhanced, closely distributed speckle patterns given by the interaction of structural features with visible light) useful for the contact-free determination of the in-plane coefficient of thermal expansion (CTE) via DIC. Two-dimensional fast Fourier transform (2D-FFT) and autocorrelations were applied to captured images to identify characteristics in the DIC speckle patterns obtained by BF, PC, and PL imaging modes. PEI, PI, and PEN films were used as case study materials due to the existence of high quality CTE data from DIC and other standard methods available for comparison. Nonetheless, the method outlined in this study could be readily extended to a large variety of polymer films and soft materials.

EXPERIMENTAL SECTION

Materials. Three different polymer films were explored: polyetherimide (PEI) (Ultem1000B, Sabic Innovative Plastics), polyethylene naphthalate (PEN) (Q65FA 500ga Teonex, DuPont Teijin Films), and polyimide (PI) (DuPont Kapton 5HN) with thicknesses of 25, 80, and 125 μm, respectively. Testing films were cut to testing dimensions (~50 × 50 mm) and thermally pretreated at 100 °C for 30 min during the first run prior to image acquisition for thermal expansion determination.

Pattern Generation and Characterization. Testing specimens were imaged in transmission mode using a Carl Zeiss (Axio Observer A1) inverted light microscope (condenser NA: 0.35, WD: 70 mm). DIC trackable patterns were obtained by studying samples under three different modes: bright field (BF) using a 5× magnification objective at low illumination, polarized light (PL) by positioning linear polarizers in extinction (i.e., 90° with respect to each other) before and after the light path of the samples, and phase contrast (PC) with a 5× phase contrast objective coupled with condenser phase stop rings within the turret disk. Characterization of the textural features (e.g., intensity and size of trackable speckle pattern) obtained by BF, PC, and PL imaging modes was completed using two-dimensional fast Fourier transforms (2D FFT) combined with autocorrelations. Images analyzed were captured for films in their reference state (i.e., at room temperature after thermal pretreatment). Fourier power spectra were calculated and azimuthally averaged for one-dimensional analysis of characteristic length-scales, and regularity,[33−36] using MatLab R2012b. Further insights about the nature of the highlighted textural features were obtained from radially averaged autocorrelations calculated with ImageJ.[37] Autocorrelation analysis was performed by describing the

dx.doi.org/10.1021/am405860y | ACS Appl. Mater. Interfaces 2014, 6, 4856−4863

decay of their normalized autocorrelation intensity as a function of distance (R) in random regions of interest (ROI) utilized in CTE calculations (Tables S1–S3). This was achieved by identifying the position of oscillations in the response, and calculating the half-width at half-maximum (HWHM), given by$(2 \ln 2\sigma)^{1/2}$.[38−40] HWHMs were calculated by fitting all autocorrelation responses to a proposed variation of the modified Gaussian function introduced by Tran et al.[34]

$$\mathrm{AC}(r) = \lambda_0 \exp\left[-\left(\frac{r}{\sqrt{2\sigma}}\right)^2\right] + \lambda_1 r^{-\lambda_2} + \lambda_3 \quad (1)$$

where mean values were shifted to $r = 0$ (i.e., maximum autocorrelation) and parameters λ_0, λ_1, λ_2, and λ_3 describe the autocorrelation decays.

In-Plane Thermal Expansion via DIC. Thermal expansion measurements were performed in a method similar to Diaz et al.[16] Measurements were performed in transmission mode by using a Carl Zeiss (Axio Observer A1) inverted microscope coupled with a heating stage (Linkam PE94). BF, PC, and PL microscopy modes were employed to generate DIC trackable patterns in PEI, PI, and PEN testing specimens as described above. After increasing film temperature at 10 °C/min and a 7 min stabilization time, 36 bit-2047 pixel × 2047 pixel images were captured at 30, 40, 60, 80, and 100 °C for PEI and PI films, and 30, 40, 50, 60, and 70 °C for PEN films, representing approximate temperature ranges of comparison to other works (Table 1). Basic processing and image conditioning (i.e., regions of interest, rotations, etc.) of all captured images were performed in both ImageJ and Adobe Photoshop. Thermal expansion calculations were performed with the open-source HighCorr package available in MathWorks, which determines thermal strains by cross-correlating sets of captured images via normalized gradients using the image toolbox in MatLab R2012b.[41,42]

■ RESULTS AND DISCUSSION

Adjusting multiple DIC parameters (i.e., subset size, number correlation points, grid spacing, etc.) over artificially applied speckle patterns has been a factor traditionally employed in DIC measurements in order to obtain better correlations between images. Here, we explored how contrast enhanced microscopy methods can generate trackable speckle patterns in images to be cross-correlated during contact-free DIC experiments of soft samples. BF, PC, and PL imaging modes were used to highlight different textures in PEI, PI, and PEN films as shown in the DIC pattern generation section. The distinctive textures obtained for all testing films were characterized by the complementary information given by Fourier and autocorrelation analyses, and employed for the determination of in-plane CTEs via two-dimensional DIC as discussed in the subsequent sections.

DIC Pattern Generation. Classical processing methods such as injection molding, film casting, and so forth typically employed in soft film manufacture generate different microstructural features mainly governed by intermolecular interactions in the bulk as during self-assembly or crystallization, as well as at interfaces as during dewetting. In polymeric systems, such characteristics are hardly resolved by naked eye (Figure 2a) and conventionally studied by SEM[43] or optical microscopy (OM). DIC relies on the cross-correlation of patterns found in two different images. Such patterns can be successfully generated by highlighting textural features from the testing specimens via OM with a maximum resolution on the order of ~0.2 μm. Likewise, regular OM low coherence light sources can be preferred to allow tracking of large deformations without disrupting sample textural features for DIC[44] or adding the need for interference fringe analysis of coherent light sources. The existence of multiple phases or aggregates in soft samples

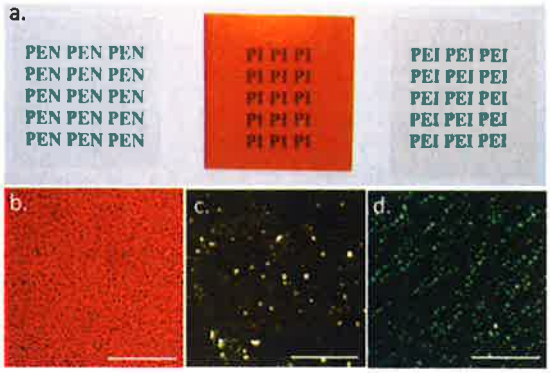

Figure 2. (a) Photograph of polyetherimide (PEI), polyimide (PI), and polyethylene naphthalate (PEN) ~5 cm × 5 cm films. (b) BF image of a PI film. (c) PC of a PEN film. (d) PL image of a PEI film. Scale bar 500 μm. Textures observed for PEI, PI, and PEN films under all microscopy modes are available in Figure S1 in Supporting Information.

will render additional textural features that can be highlighted by different imaging modes; thus, the technique can remain invariant and likely be benefited as the complexity of the specimen increases. Thus, artificially introduced patterns and further image contrast enhancement can be practically eliminated by controlling saturation, reflection, and contrast from the microscopy mode itself as shown in Figure 2b–d.

Textures imaged by BF are partially limited to the interaction of visible light with present microstructural features or thickness profiles. Although BF follows in principle the customary light path DIC methodology, the selected magnification together with image quality can accentuate features that render a broader number of grayscale values. The high intensity illumination more easily achieved in BF can be very advantageous to highlight textural features in films with relatively high thickness, reduced optical clarity, or colored appearances as in the case of PI films (Figure 2b).

Much higher contrast can be obtained in PC and PL imaging modes as shown in Figure 2c and d, respectively. PC increases contrast by transforming light phase shifts through the sample into brightness variations (Figure 2c), and in contrast to PL, the resultant texture does not rely on domain orientations. Because of this, PC allows the ability to create contrast in samples without structured crystalline domains. For example, in the case of biaxially oriented PEN films,[45] whose textures imaged by bright field or polarized light would highlight only minimal textural features, phase contrast represented a more efficient way of distinguishing trackable patterns for DIC (see Figure S1).

PL is similar to PC in that it also increases image contrast but the working principle is different. PL reveals textural features related to domain orientations, and thickness gradients present in the samples as a function of the angle between polarizers (Figure S2 in Supporting Information for PL patterns obtained for ultrahigh molecular weight polyethylene, and cellulose nanocrystals). Hence, PL can be highly beneficial for regions exhibiting different refractive indices[16,32] or even tracking crystalline areas embedded within amorphous regions. For example, within the explored films, polarized light highlighted distinctive textures in PEI films, which were homogeneously distributed over the entire film (Figure 2d), as opposite to the plain responses obtained for PI or PEN films (Figure S1). In all imaging modes the presence of defects, coatings, or impurities

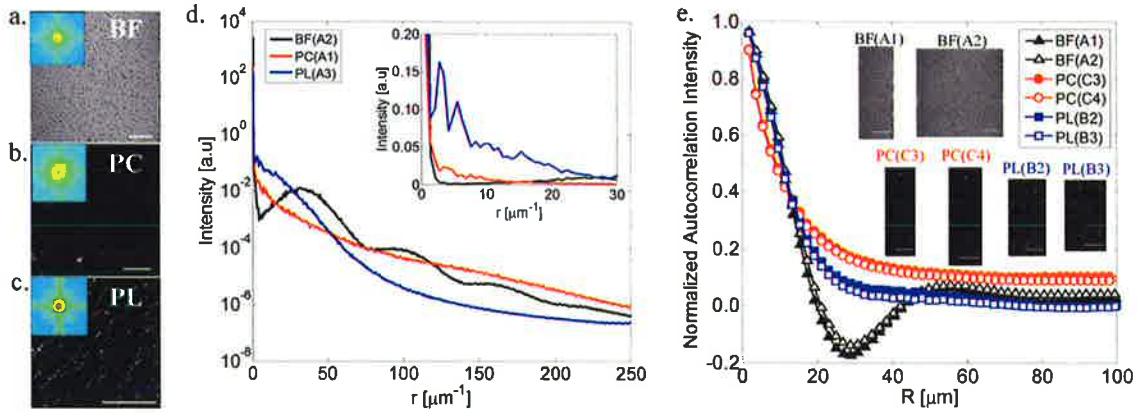

Figure 3. Bright field (BF), phase contrast (PC), and polarized light (PL) microscopy images of polyether imide (PEI) films (a, b, c) with their respective 2D-FFT power spectra (insets) and azimuthally averaged one-dimensional Fourier spectra with removal of zero wavevector shown in inset at low reciprocal space values (d). (e) One-dimensional normalized autocorrelation intensity for BF, PC, and PL microscopy images of PEI films applied to different regions of interest (ROIs) per mode (BF(A1), PC(C3), etc.). Detailed information on all ROIs is available in Tables S1–S3, Figure S5. Scale bar = 500 μm.

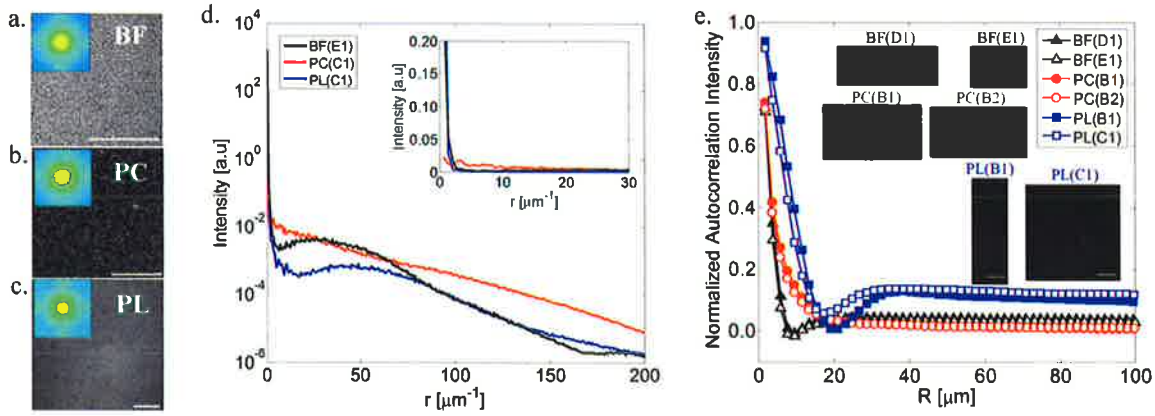

Figure 4. Bright field (BF), phase contrast (PC), and polarized light (PL) microscopy images of polyimide (PI) films (a, b, c) with their respective 2D-FFT power spectra (insets) and azimuthally averaged one-dimensional Fourier spectra with removal of zero wavevector shown in inset at low reciprocal space values (d). (e) One-dimensional normalized autocorrelation intensity for BF, PC, and PL microscopy images of PI films applied to different regions of interest (ROIs) per mode (BF(D1), PC(B1), etc.). Detailed information on all ROIs is available in Tables S1–S3, Figure S5. Scale bar = 500 μm.

from manufacturing and manipulation of the samples will affect the resultant texture of the images to be cross-correlated in DIC as discussed in the next sections.

Textural Characterization. The characterization of distinctive textures in testing images becomes particularly relevant during CTE calculations of non-artificially speckled samples, as textural features have been found to affect the cross-correlation of peaks[46] and play a major role during DIC measurements.[46−48] Different approaches could be considered to describe image patterns, some based on image thresholding (e.g., global mean speckle size,[48] Shannon entropy[46]) and others on local morphology analysis like Laplacian of Gaussian edge detection:[46] all meaning to describe the speckle characteristics within the images to be correlated. Here, we employ Fourier analysis (broadly used to analyze microstructural features in various soft materials such as collagen fibers present in biological tissues[49] and changes in morphology in polymer blends[33,34]) complemented by autocorrelations to describe the main textural features and possible repetitive patterns[40,50,51] obtained for PEI, PI, and PEN films under BF, PC, and PL modes at fixed 5× magnification. This approach is suggested as an integral description of the variety of textural features present in polymer films, that can represent viable options to the conventional speckle patterns employed in DIC measurements, and further CTE calculation in complex testing systems.

PEI films imaged in BF exhibited a spinodal ring in the power spectrum (Figure 3a, inset) generated by the granular-like texture present in the real space image (Figure 3a), extended to different lengths (Figure 3d). Autocorrelations performed in some representative ROIs (Figure 3e) indicated the presence of anti-correlations (negative values),[37] and speckles with sizes around 31 μm and interspacing distances on the order of 60 μm (position of the first minimum and first maximum, respectively).[38] The global response for PEI films under BF was therefore governed by a distribution of low contrast, repetitive small features (HWHM ~10.3 ± 0.5 μm) throughout the images. PC highlighted high contrast and sparsely distributed random spots over PEI films (Figure 3b). The combination of such factors in the texture was observed with plain responses observed in its respective 1D and 2D power spectra (Figure 3b (inset) and d) as well as autocorrelations (Figure 3e) with large variations in textures given by variable highlighted patterns (HWHM ~13.8 ± 2.2 μm, features

dx.doi.org/10.1021/am405860y | ACS Appl. Mater. Interfaces 2014, 6, 4856−4863

ranging from 35 to 80 μm). PL imaging of PEI films highlighted a distinctive speckle pattern with high contrast, and a close periodic distribution of sizes as seen in Figure 3c and d. Based on the autocorrelations, PL imaging exhibited more uniform responses than images taken in PC mode, also yielding an average HWHM with lower standard deviation, 10.9 ± 0.2 μm, and lowering feature size to ~30 μm (Figure 3e).

In general, PI films exhibited much finer texture than PEI films in all imaging modes, which can also be observed from the plain response in their power spectra and autocorrelations. PI films imaged under BF generated a low contrast 2D power spectrum that only exhibited small features located at low frequencies (Figure 4a,d). An autocorrelation average HWHM of 4.4 ± 1.2 μm for different ROIs also confirmed the rapid decay and fine morphology with features size ranging from 10 to 20 μm, and spacing on the order of 25 μm (Figure 4e). The contrast enhancement provided by PC generated low intensity, finely speckled patterns as shown in Figure 4b, with autocorrelations revealing better pattern uniformity than that obtained for PEI films, and small feature sizes ~20 μm, HWHM ~6.3 ± 0.7 μm. Due to the absence of distinctive thicknesses gradients and orientational domains in PI films (Figure 4c), the textural response under PL (Figure 4d) exposed minimal features closely approaching the one exhibited under BF, with fine textures (~15 μm, HWHM ~5.8 ± 1.0 μm) and larger spacing distances ~30 μm (Figure 4e). The performance exhibited by PEN films in phase contrast can be seen in Figures S3 and S4 in Supporting Information.

Thermal Expansion of Polymer Films. The in-plane coefficients of thermal expansion (CTEs) were calculated from 30 to 100 °C for PI and PEN films, and from 30 to 70 °C for PEI films. Temperature ranges were selected to prevent humidity effects below 30 °C, and reduce light distortions from out-of-plane CTEs, while still being representative of the thermal expansion of the polymers. Full field displacement measurements of the polymer films were achieved since BF, PC, and PL imaging highlighted textures where the cross-correlated intensity peaks calculated by normalized gradients had non-zero standard deviations within selected subsets.[41,42] Detailed explanation of DIC algorithms can be reviewed elsewhere.[46,48] Thermal strains can be calculated in multiple directions due to the full field nature of DIC. Such a characteristic becomes very important in materials exhibiting structural anisotropy (Figure S2 in Supporting Information), as polarized light can contrast different regions based on orientations to estimate displacements.[16,32] ROIs in PI, PEI, and PEN films were cross-correlated using different subsets sizes (Tables S1–S3) with respect to the first image (i.e., image taken at 30 °C). Subsets of 60 pixels provided balance between accuracy and computation times as subsets of 30 pixels decreased correlation times and accuracy of the results, and subsets of 90 pixels increased correlation times above 10 min per run with minimal improvement of image correlations. Figure 5a–c shows the thermal strain in the axial (x) and transverse (y) directions of some representative testing films as a function of temperature and imaging mode, where CTEs were calculated as the slope of the curves after linear fitting the strain responses over entire temperature ranges and summarized in Table 1.

ROIs for CTE calculations were randomly distributed in different polymer samples (Figures 5, Tables S1–S3, Figure S6) in order to better gauge the thermal response of the films. As DIC parameters remained constant during thermal expansion

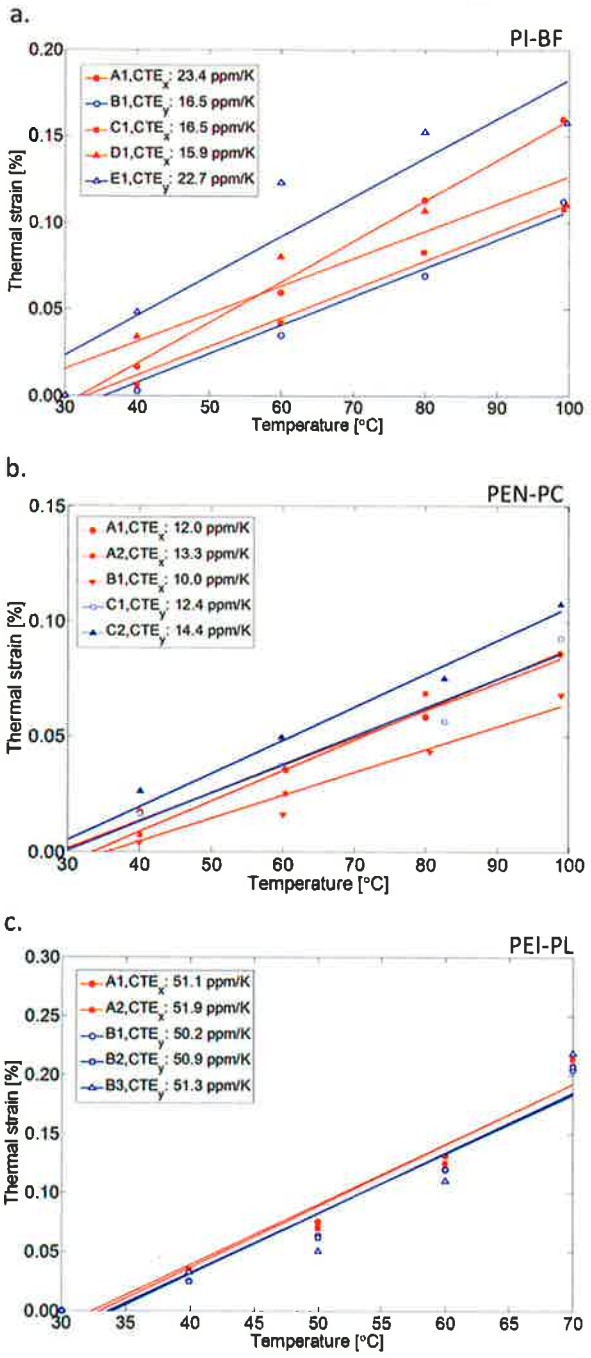

Figure 5. Thermal strain vs temperature plots calculated for different ROIs (A1, B1, etc.) in (a) PI films in bright field (b) PEN films in phase contrast and (c) PEI films in polarized light. Performance exhibited for all films imaged in other modes can be seen Figure S6 and Tables S1–S3 in Supporting Information.

calculations and assuming minimal anisotropic expansion gradients during thermal loads, imaging modes tended to provide similar standard deviations (~3.0 ppm/K) created by differences in highlighted natural textures. Although different textural features were obtained from imaged specimens as analyzed by Fourier and autocorrelation treatments, PEI, PI, and PEN films exhibited isotropic thermal responses (Table 1) that closely approached those determined by using DIC with artificial speckle patterns[13,15] or other standard methods[45,52,53] that are available in the literature. Thus, areas containing different textural features, under fixed magnification, can yield

dx.doi.org/10.1021/am405860y | ACS Appl. Mater. Interfaces 2014, 6, 4856–4863

close cross-correlations between images that maintain good precision during CTE determination.

PC provided high contrast images with relatively large speckle sizes (Figure 2c, Table 1) which, in turn, can reduce the randomness of the patterns.[46] Conversely, BF yielded a lower distribution of grayscale levels with closely distributed textural features (Figures 3a, 4a, Table 1). A less generalized response can be found for materials imaged by polarized light, as the response is highly dependent on the material (Table 1); for instance, high contrast regions with dense distribution can be found for PEI films (Figure 3c), whereas an opposite response is found in other materials like in PI films (Figure 4c). Although cross-correlation of images of PI films can be potentially increased by the presence of fine speckle patterns observed under BF, PC, and PL, it will also be decreased due to low contrast enhancement achieved in all imaging modes, aspect that can be identified a priori. The method illustrated here using PEI, PI, and PEN films as standard materials can be further enhanced by the introduction of wave plates, change of type of polarizers (i.e., circular, elliptical) or increase in magnification, and readily extended to other type of materials in reflection mode. Likewise, the contact-free determination of thermal strains at high temperatures (e.g., glass transitions, softening or degradation points) and hygroscopic deformations represent natural extensions of the proposed approach as long as the generated textural features are preserved during the experimental interval studied. A preliminary estimation of the success of the technique, and the possible need for further DIC parameter adjustments, can be achieved by a quick examination or analysis of the textural features (e.g., feature size, abundance, contrast) highlighted in the testing samples by a particular imaging approach.

In cases with larger variations in texture between modes like in ultrahigh molecular weight polyethylene (Figure S2 Supporting Information), typical DIC parameters within the cross-correlation algorithm like subset size and grid spacing become more relevant to properly track the displacement of grayscale intensities.[29,48] Image distortions close to the edges, minimal friction at specimen heating-stage interface, and out-of-plane thermal expansion of samples are not entirely removed and could affect the reproducibility of the thermal expansion experiments,[14] but could also be substantially minimized by selecting central regions of interest for correlations, preheating the sample during first run, and reducing image magnifications. Illumination is also a relevant factor during image capturing as the image intensity can affect the quality of the correlation.[4,30,44] For all testing specimens, high intensity from light source improved image contrast in PC mode, but the formation of halos can limit the resolution. In BF and PL modes, the effect of increasing light intensity was not as beneficial as intensity gradients tended to be planarized, which allows for a less precise correlation of pixel intensity among images.

Although the microstructural features present in soft materials are given by several factors, textural features highlighted for DIC measurements can be controlled and improved by the imaging method employed (i.e., PC, PL, etc.). Depending on the type of soft material analyzed, the structures will exhibit different distributions of speckle patterns visualized under different modes and conventional DIC parameters (e.g., subset size, number of correlation points) can be adjusted to properly determine strains in the system. The resolution in CTE calculation via DIC could be reduced (Figure 1) due to the random appearance of textural features (i.e., regions lacking distinctive textures like PEN films imaged by BF and PL; Figure S1); nonetheless, a contact-free characterization of delicate samples can be obtained, hence achieving a more complete description of their fundamental properties.

CONCLUSIONS

We described an inexpensive and practical method to generate textures that can be subsequently used in digital image correlation (DIC) (e.g., fine, contrast enhanced, speckle-like patterns) for the determination of thermal expansion in soft films. Textural features suitable for DIC were produced in a contact-free fashion by using bright field and contrast enhanced optical microscopy modes (i.e., polarized light, and phase contrast). The resulting textural features were characterized by Fourier and autocorrelation analyses in terms of fineness, intensity gradients, and pattern distributions. Three polymer films were investigated: polyetherimide (PEI), polyimide (PI), and polyethylene naphthalate (PEN). The resulting DIC in-plane coefficients of thermal expansion (CTE) calculated using contrast enhanced optical microscopy patterns were comparable to those previously reported with artificially applied speckle patterns. The method outlined in this study could be readily extended to and is optimal for determination of anisotropic strain fields in samples too delicate for applied speckle patterns (i.e., solvent-sensitive, self-standing thin films, porous materials, etc.) where conventional testing methods remain limited.

ASSOCIATED CONTENT

Supporting Information

PEI, PI, and PEN films imaged under BF, PC, and PL. Polarized light patterns obtained for ultrahigh molecular weight polyethylene and a cellulose nanocrystal film. Fourier and autocorrelation analyses of polyethylene naphthalate (PEN) films under phase contrast. Tables of DIC parameters employed for CTE calculation in polymer films for all imaging modes. This material is available free of charge via the Internet at http://pubs.acs.org.

AUTHOR INFORMATION

Corresponding Author

*E-mail: jpyoungb@purdue.edu.

Notes

The authors declare no competing financial interest.

ACKNOWLEDGMENTS

The authors would like to thank the Air Force Office of Scientific Research grant #FA9550-11-1-0162 for supporting this project, and Prof. Carlos Martinez (Purdue University) for valuable discussions.

REFERENCES

(1) Parsons, E.; Boyce, M. C.; Parks, D. M. An Experimental Investigation of the Large-Strain Tensile Behavior of Neat and Rubber-Toughened Polycarbonate. *Polymer* **2004**, *45*, 2665−2684.

(2) Sun, Z.; Lyons, J. S.; McNeill, S. R. Measuring Microscopic Deformations with Digital Image Correlation. *Opt. Lasers Eng.* **1997**, *27*, 409−428.

(3) Scrivens, W. A.; Luo, Y.; Sutton, M. A.; Collette, S. A.; Myrick, M. L.; Miney, P.; Colavita, P. E.; Reynolds, A. P.; Li, X. Development of Patterns for Digital Image Correlation Measurements at Reduced Length Scales. *Exp. Mech.* **2007**, *47*, 63−77.

(4) Berfield, T. A.; Patel, J. K.; Shimmin, R. G.; Braun, P. V.; Lambros, J.; Sottos, N. R. Micro- and Nanoscale Deformation

Measurement of Surface and Internal Planes via Digital Image Correlation. *Exp. Mech.* **2007**, *47*, 51−62.
(5) Lagattu, F.; Bridier, F.; Villechaise, P.; Brillaud, J. In-Plane Strain Measurements on a Microscopic Scale by Coupling Digital Image Correlation and an in Situ SEM Technique. *Mater. Charact.* **2006**, *56*, 10−18.
(6) Chasiotis, I.; Knauss, W. G. A New Microtensile Tester for the Study of MEMS Materials with the Aid of Atomic Force Microscopy. *Exp. Mech.* **2002**, *42*, 51−57.
(7) Xu, Z.-H.; Li, X.-D.; Sutton, M. A; Li, N. Drift and Spatial Distortion Elimination in Atomic Force Microscopy Images by the Digital Image Correlation Technique. *J. Strain Anal. Eng. Des.* **2008**, *43*, 729−743.
(8) Beaucage, G.; Composto, R.; Stein, R. S. Ellipsometric Study of the Glass Transition and Thermal Expansion Coefficients of Thin Polymer Films. *J. Polym. Sci., Part B: Polym. Phys.* **1993**, *31*, 319−326.
(9) Hagy, H. E. High Precision Photoelastic and Ultrasonic Techniques for Determining Absolute and Differential Thermal Expansion of Titania-Silica Glasses. *Appl. Opt.* **1973**, *12*, 1440−1446.
(10) Dudescu, C.; Naumann, J.; Stockmann, M.; Nebel, S. Characterisation of Thermal Expansion Coefficient of Anisotropic Materials by Electronic Speckle Pattern Interferometry. *Strain* **2006**, *42*, 197−205.
(11) Kim, K.; Kim, J.; Lee, J.; Jarng, S. Measurement of Thermal Expansion Coefficients by Electronic Speckle Pattern Interferometry at High Temperature. *J. Mater. Sci. Lett.* **1997**, *16*, 1753−1756.
(12) Su, C.-H.; Feth, S.; Lehoczky, S. L. Thermal Expansion Coefficient of ZnSe Crystal between 17 and 1080 °C by Interferometry. *Mater. Lett.* **2009**, *63*, 1475−1477.
(13) Liu, Z.; Gao, J. Deformation-Pattern-Based Digital Speckle Correlation for Coefficient of Thermal Expansion Evaluation of Film. *Opt. Express* **2011**, *19*, 17469−17479.
(14) Wang, Y. G.; Tong, W. A High Resolution DIC Technique for Measuring Small Thermal Expansion of Film Specimens. *Opt. Lasers Eng.* **2013**, *51*, 30−33.
(15) Van den Berg, D.; Barink, M.; Giesen, P.; Meinders, E.; Yakimets, I. Hygroscopic and Thermal Micro Deformations of Plastic Substrates for Flexible Electronics Using Digital Image Correlation. *Polym. Test.* **2011**, *30*, 188−194.
(16) Diaz, J. A.; Wu, X.; Martini, A.; Youngblood, J. P.; Moon, R. J. Thermal Expansion of Self-Organized and Shear-Oriented Cellulose Nanocrystal Films. *Biomacromolecules* **2013**, *14*, 2900−2908.
(17) Wada, M. Lateral Thermal Expansion of Cellulose I_β And III_I Polymorphs. *J. Polym. Sci., Part B: Polym. Phys.* **2002**, *40*, 1095−1102.
(18) Olmos, D.; Martínez, F.; González-Gaitano, G.; González-Benito, J. Effect of the Presence of Silica Nanoparticles in the Coefficient of Thermal Expansion of LDPE. *Eur. Polym. J.* **2011**, *47*, 1495−1502.
(19) Zhang, X. R.; Fisher, T. S.; Raman, A.; Sands, T. D. Linear Coefficient of Thermal Expansion of Porous Anodic Alumina Thin Films from Atomic Force Microscopy. *Nanoscale Microscale Thermophys. Eng.* **2009**, *13*, 243−252.
(20) Sao, G. D.; Tiwary, H. V. Thermal Expansion of Poly(vinylidene Fluoride) Films. *J. Appl. Phys.* **1982**, *53*, 3040−3043.
(21) Tong, H. M.; Hsuen, H. K. D.; Saenger, K. L.; Su, G. W. Thickness-Direction Coefficient of Thermal Expansion Measurement of Thin Polymer Films. *Rev. Sci. Instrum.* **1991**, *62*, 422−430.
(22) De Lima, M. M.; Lacerda, R. G.; Vilcarromero, J.; Marques, F. C. Coefficient of Thermal Expansion and Elastic Modulus of Thin Films. *J. Appl. Phys.* **1999**, *86*, 4936−4942.
(23) Fang, W.; Lo, C. On the Thermal Expansion Coefficients of Thin Films. *Sens. Actuators* **2000**, *84*, 310−314.
(24) ASTM Standard E 831-12, Test Method for Linear Thermal Expansion of Solid Materials by Thermomechanical Analysis. *Am. Soc. Test. Mater.*, 2012.
(25) IPC-TM-650, Test Method to Determine Glass Transition Temperature and Coefficient of Thermal Expansion of Materials Used in High Density Interconnection and Microvias. TMA Method. *Inst. Interconnecting Packag. Electron. Circuits*, 1998.
(26) ASTM E 228-11, Test Method for Linear Thermal Expansion of Solid Materials with a Push-Rod Dilatometer. *Am. Soc. Test. Mater.*, 2011.
(27) Adams, D. F.; Carlsson, L. A.; Pipes, R. B. *Experimental Characterization of Advanced Composite Materials*, 3rd ed.; CRC Press: Boca Raton, 2003; pp 143−149 and 163−167.
(28) ASTM E 289-04 (Reapproved 2010), Test Method for Linear Thermal Expansion of Rigid Solids with Interferometry. *Am. Soc. Test. Mater.*, 2010.
(29) Pan, B.; Qian, K.; Xie, H.; Asundi, A. Two-Dimensional Digital Image Correlation for In-Plane Displacement and Strain Measurement: A Review. *Meas. Sci. Technol.* **2009**, *20*, 062001.
(30) Zhang, D.; Luo, M.; Arola, D. D. Displacement/strain Measurements Using an Optical Microscope and Digital Image Correlation. *Opt. Eng.* **2006**, *45*, 033605.
(31) Rae, P. J.; Palmer, S. J.; Goldrein, H. T.; Lewis, A. L.; Field, J. E. White-Light Digital Image Cross-Correlation (DICC) Analysis of the Deformation of Composite Materials with Random Microstructure. *Opt. Lasers Eng.* **2004**, *41*, 635−648.
(32) Skulborstad, A. J.; Wang, Y.; Davidson, J. D.; Swartz, S. M.; Goulbourne, N. C. Polarized Image Correlation for Large Deformation Fiber Kinematics. *Exp. Mech.* **2013**, *53*, 1405−1413.
(33) Nisato, G.; Ermi, B. D.; Douglas, J. F.; Karim, A. Excitation of Surface Deformation Modes of a Phase-Separating Polymer Blend on a Patterned Substrate. *Macromolecules* **1999**, *32*, 2356−2364.
(34) Tran-Cong-Miyata, Q.; Nishigami, S.; Ito, T.; Komatsu, S.; Norisuye, T. Controlling the Morphology of Polymer Blends Using Periodic Irradiation. *Nat. Mater.* **2004**, *3*, 448−451.
(35) Fujita, T.; Chen, M. W. Characteristic Length Scale of Bicontinuous Nanoporous Structure by Fast Fourier Transform. *Jpn. J. Appl. Phys.* **2008**, *47*, 1161−1163.
(36) Fujiki, D.; Jing, C.; Van-Pham, D.-T.; Nakanishi, H.; Norisuye, T.; Tran-Cong-Miyata, Q. Polymer Materials with Spatially Graded Morphologies: Preparation, Characterization and Utilization. *Adv. Nat. Sci. Nanosci. Nanotechnol.* **2011**, *1*, 043003.
(37) ImageJ wiki. http://imagejdocu.tudor.lu/doku.php?id=macro:radially_averaged_autocorrelation; Accessed September 5, 2013.
(38) Wang, D.; Ji, R.; Schaaf, P. Formation of Precise 2D Au Particle Arrays via Thermally Induced Dewetting on Pre-Patterned Substrates. *Beilstein J. Nanotechnol.* **2011**, *2*, 318−326.
(39) Bornert, M.; Brémand, F.; Doumalin, P.; Dupré, J.-C.; Fazzini, M.; Grédiac, M.; Hild, F.; Mistou, S.; Molimard, J.; Orteu, J.-J.; Robert, L.; Surrel, Y.; Vacher, P.; Wattrisse, B. Assessment of Digital Image Correlation Measurement Errors: Methodology and Results. *Exp. Mech.* **2008**, *49*, 353−370.
(40) Rubin, D. M. A Simple Autocorrelation Algorithm for Determining Grain Size from Digital Images of Sediment. *J. Sediment Res.* **2004**, *74*, 160−165.
(41) Thompson, R.; Hemker, K. Thermal Expansion Measurements on Coating Materials by Digital Image Correlation. *Proc. SEM Conf. Exp. Mech.* **2007**, *2*, 1058−1067.
(42) MatWorks. http://www.mathworks.com/matlabcentral/fileexchange; Accessed October 15, 2012.
(43) Vesely, D. Microstructural Characterization of Polymer Blends. *Polym. Eng. Sci.* **1996**, *36*, 1586−1593.
(44) Reu, P. Stereo-Rig Design: Lighting-Part 5. *Exp. Tech.* **2013**, *37*, 1−2.
(45) MacDonald, W. Engineered Films for Display Technologies. *J. Mater. Chem.* **2004**, *14*, 4−10.
(46) Crammond, G.; Boyd, S. W.; Dulieu-Barton, J. M. Speckle Pattern Quality Assessment for Digital Image Correlation. *Opt. Lasers Eng.* **2013**, *51*, 1368−1378.
(47) Pan, B.; Lu, Z.; Xie, H. Mean Intensity Gradient: An Effective Global Parameter for Quality Assessment of the Speckle Patterns Used in Digital Image Correlation. *Opt. Lasers Eng.* **2010**, *48*, 469−477.
(48) Lecompte, D.; Smits, A.; Bossuyt, S.; Sol, H.; Vantomme, J.; Van Hemelrijck, D.; Habraken, A. M. Quality Assessment of Speckle

Patterns for Digital Image Correlation. *Opt. Lasers Eng.* **2006**, *44*, 1132−1145.
(49) Schriefl, A. J.; Reinisch, A. J.; Sankaran, S.; Pierce, D. M.; Holzapfel, G. A. Quantitative Assessment of Collagen Fibre Orientations from Two-Dimensional Images of Soft Biological Tissues. *J. R. Soc. Interface* **2012**, *9*, 3081−3093.
(50) Heilbronner, R. P. The Autocorrelation Function: An Image Processing Tool for Fabric Analysis. *Tectonophysics* **1992**, *212*, 351−370.
(51) Taylor, V. L.; Costello, M. J. Fourier Analysis of Textural Variations in Human Normal and Cataractous Lens Nuclear Fiber Cell Cytoplasm. *Exp. Eye Res.* **1999**, *69*, 163−174.
(52) DuPont Kapton HN Film. Technical Data Sheet.
(53) Sabic Innovative Plastics. Product Datasheet Ultem*1000B Natural Film.